Direct mechanosynthesis of pure $BiFeO_3$ perovskite nanoparticles: reaction mechanism.

Antonio Perejón [a], Nataliya Murafa[b], Pedro E. Sánchez-Jiménez[a], José M. Criado[a], Jan Subrt[b], María J. Diánez[a], Luis A. Pérez-Maqueda*[a]

In this work, a mechanochemical procedure is proposed as a simple and fast method to synthesize pure $BiFeO_3$ perovskite phase as a nanostructured material without the need for purification treatments, while the mechanochemical reaction mechanism has been investigated and correlated with that of the conventional solid-state reaction. Thus, different milling conditions have been used as a tool for tailoring the crystallite size of the resulting $BiFeO_3$ nanoparticles. The materials prepared by mechanochemical reaction could be annealed or sintered without the formation of unwilling phases. Both the ferroelectric and ferromagnetic transitions were observed by DSC. Finally, the dielectric constants at different frequencies as a function of the temperature for the prepared material have been measured, showing that the material is clearly an isolator below 200ºC, characteristic of a high quality $BiFeO_3$ material.

Introduction

Multiferroics, by the original definition, are materials which combine two or more "ferroic" properties in the same phase: ferroelectricity, ferromagnetism and ferroelasticity. However, the possibility of ferrotoroidic order is included and the classification of a multiferroic has been broadened to include antiferroic order.[1] Among them, magnetoelectric materials are those which present an induction of a magnetization by an electric field or a polarization by a magnetic field. This compounds have attracted great attention in recent years, because of their physical properties, that becomes these compounds potential candidates for technical applications such as data storage, spintronics, sensors, etc.[2, 3]

Perovskites have been considered as the most promising multiferroic materials because many of them are magnetic or ferroelectric. However, only a few of stoichiometric perovskites present both properties at the same time.[4] $BiFeO_3$ is one of these compounds, which presents multiferroic properties at room temperature, making it one of the most studied multiferroics. $BiFeO_3$ is reported to present a rhombohedrally distorted perovskite structure at room temperature with space group R3c. It shows a G-type antiferromagnetic behavior below its Néel temperature (T_N ~ 360 ºC) and is ferroelectric below its Curie temperature (Tc ~ 830ºC). [5-8]

[a] Instituto de Ciencia de Materiales de Sevilla (C.S.I.C. – Univ. Sevilla), Américo Vespucio 49, Sevilla 41092, Spain

[b] Institute of Inorganic Chemistry AS CR, 250 60 Řež, Czech Republic.

Many attempts have been made in order to obtain a pure phase in bulk of $BiFeO_3$ by means of numerous different processes, i.e. solid state reactions,[9-14] wet chemical synthesis including sol-gel methods with the use of polymeric precursors,[15-20] solution combustion methods,[21, 22] mechanical activation,[23] mechanochemical synthesis,[24-26] hydrothermal synthesis,[27-30] using molten salts,[31, 32] and others, including combinations of these methods. However, pure $BiFeO_3$ in bulk has been obtained only in special synthesis conditions because it is difficult to avoid the formation of small amounts of impurity phases, mainly $Bi_{25}FeO_{39}$ and $Bi_2Fe_4O_9$,[11, 21] although other phases could appear due to non-suitable preparation methods or an improper control of the experimental conditions. For instance, the $Bi_{36}Fe_2O_{57}$ phase has been found in samples prepared by conventional solid state synthesis and in fibers prepared by sol-gel methods.[33-35] The $Bi_{46}Fe_2O_{72}$ phase was detected in samples prepared by conventional solid state synthesis and in nanoparticles obtained by sol-gel.[34, 36] Both phases were also observed by Yuan et al.[37] The phase diagram proposed for the system Bi_2O_3-Fe_2O_3 shows that $BiFeO_3$ is formed in a narrow range of compositions and, even, it has been argued that $BiFeO_3$ is thermodynamically metastable in air[12, 38, 39] and that its dissociation temperature is lower than its formation temperature.[40] Researchers have suggested different reasons for the formation of secondary phases, but how these phases are formed during the synthesis or during thermal treatments are still under debate.

Several authors have reported that oxygen vacancies play an important role in the formation of deoxygenated impurities and

Table 1. Experimental conditions used for the different milling experiments.

Experimental conditions	Rotational speed (rpm)	Jar radius (mm)	Ball diameter (mm)	Ball material	Ball-to powder mass ratio	Corrected impact energy (mJ hit^{-1})	Power (W)
1	700	19.8	15	Hardened Steel	20:1	60	12.6
2	650	23.2	15	Hardened Steel	20:1	71	20.7
3	700	23.2	15	Hardened Steel	20:1	82	25.8
4	700	26.5	15	Hardened Steel	20:1	109	34.3
5	700	26.5	16	Tungsten Carbide	40:1	230	72.6
6	650	37.7	16	Tungsten Carbide	40:1	377	355

.

have found that they are the main cause of low electrical resistivity and high porosity in the multi-phase synthesized samples.[37, 41] In this sense, Yuan et al[37] and Selbach el al[42] have studied the influence of the partial pressure of oxygen in the stabilization of the $BiFeO_3$ phase. They have proposed that the phase relations near $BiFeO_3$ depends strongly on oxygen pressure and by DTA have determined that $BiFeO_3$ is more stable in O_2 than in N_2 atmosphere, thus a higher partial pressure of oxygen could stabilize $BiFeO_3$.

Recently, it has been reported that nanostructured (0D and 1D) multiferroic materials show improved properties as compared with bulk ones. Thus, Chen et al have found that the dielectric constant of $BiFeO_3$ pellets prepared from nanoparticles is much higher than the values previously reported for ceramics and films.[31] Moreover, for this material, it has been described a size-dependent magnetic behavior. Thus, Park et al have observed increased magnetization values at the nanoscale[43] while Mazumder et al have reported that nanoscale $BiFeO_3$ depicts not only high saturation magnetization but genuine ferromagnetic behavior with finite coercivity at room temperature.[44] Da Silva et al have shown that $BiFeO_3$ nanoparticles exhibit enhanced magnetization, enhanced coercivity, and shifted hysteresis loop.[26] Additionally, it has been described that the Néel temperature decreases with decreasing the crystallite size.[19, 45] Finally, it has been confirmed the presence of strong multiferroic coupling in nanometric $BiFeO_3$ and thus those nanoparticles are expected to be more useful for magnetoelectric device applications.[45]

Mechanochemical processes produce nanostructured materials by using mechanical energy to activate chemical reactions and structural changes as well as particle reduction.[46] Thus, this has become a popular method to make nanocrystalline materials because of its simplicity, the relative inexpensive equipment needed and the applicability to essentially all classes of materials, existing the possibility to scale up to tonnage quantities of material for various applications.[47] It has been shown that, by high energy mechanochemical milling process, some ferroelectric materials can be synthesized directly from their oxide precursors in the form of nano-sized powders, without the need for calcination at intermediate temperatures, thus making the process very simple and cost-effective.[48] Various ferroelectric compounds have been produced via the high-energy mechanical milling processes, as barium titanate and barium titante composites,[49, 50] lead titanate[51] and lead lanthanum zirconate titanate.[52] The mechanochemical synthesis of $BiFeO_3$[24-26] has been also reported in literature, but the study of the factors influencing the kinematic of the mill on the reaction kinetic as well as the study mechanism of the reaction induced by mechanical treatment are still missing.

The objective of this work is to explore the mechanochemical synthesis as a general, simple and reproducible method to synthesize pure nanostructured $BiFeO_3$ paying special attention to the mechanism of the solid-state reactions involved, the presence of intermediates and the formation of the final $BiFeO_3$ nanoparticles. Additionally, the control of the crystallite size of the products by means of selecting milling conditions will be investigated.

Experimental section

Sample preparation

The samples were prepared from commercially available oxides: Bi_2O_3 (Sigma-Aldrich 223891-500G, 10 μm, 99.9% in purity) and Fe_2O_3 (Sigma-Aldrich 310050-500G, <5 μm, ≥99% in purity). This purity refers to maximum deviation from stoichiometry provided that both iron and bismuth have variable valence, but the starting materials used only contain traces of other metals. Stoichiometric amounts of the oxides were mechanically treated under different milling conditions, i.e. milling energy, reaction time and grinding atmosphere. Two different planetary mills were used, i.e. Pulverisette 7 (Fritsch) and PM100 (Retsch). Both mills were modified by incorporating a rotary valve that allows connecting the stainless steel jar (sealed with a Viton o-ring and equipped with a male taper straight adaptor) and the gas cylinder during milling experiment. Thus, the pressure inside the jar could be maintained constant during the entire treatment even if the gas is consumed in the reaction. In all experiments, the jars were purged several times with the selected gas and then the desired pressure was selected and maintained during milling. The influence of the atmosphere in the grinding products was investigated by performing experiments under static air, nitrogen and oxygen.

To study the influence of milling conditions on the reaction of

formation of $BiFeO_3$, different experiments were performed using either stainless steel balls or tungsten carbide balls (table 1). The powder-to-ball mass ratio was set at 1:20 for stainless steel balls and at 1:40 for tungsten carbide balls. Thus, the empty-to-filled volume ratio inside the jar was identical for the whole set of experiments. The influence of the milling power on the reaction was investigated by modifying the jar diameter.

Characterization

X-ray diffraction patterns were collected with a Panalytical X'Pert Pro diffractometer working at 45 kV and 40 mA, using $CuK_{\alpha 1,2}$ radiation and equipped with a X'Celerator detector and a graphite diffracted beam monochromator. The sizes of coherently diffracting domains and strain contents were calculated from the (024) diffraction peak by the line profile analysis procedure (Panalytical X'Pert Pro software) corrected for instrumental peak broadening determined with a silicon standard. Elemental composition of the samples was assayed by X-ray fluorescence analysis using an Axios XRF Spectrometer (Panalytical) equipped with a Rh tube.

The FullProf software was used for Rietveld refinements.[53, 54] The background was refined using a six-order polynomial function and a pseudo-Voigt with axial divergence asymmetry profile function was used to refine the shapes of the $BiFeO_3$ peaks. The space group R3c was used as a model, with the starting values of lattice parameters and atomic positions adopted from Moreau et al.[8] Peak shapes, lattice parameters, and scale were refined simultaneously. Atomic positions and isotropic temperature factors were included in the refinement after convergence.

Raman spectra were collected with a dispersive Horiva Jobin Yvon LabRam HR800 microscope with a 20 mW green laser (532.14 nm) and using a 100× objective with a confocal pinhole of 10 μm.

The X-ray Photoelectron Spectra (XPS) were recorded with a Vacuum Generators, model Escalab 210, equipment by using a Mg K_α calibrated with C_{1s} signal, with a pass energy resolution of 50 eV. The spectra of the powder sample were recorded at room temperature under a residual pressure lower than 10^{-10} mbar.

The microstructure of the powders was studied by scanning electron microscopy (SEM) and high-resolution transmission electron microscopy (HRTEM). SEM micrographs were obtained in a Hitachi S-4800 microscope equipped with energy dispersive X-ray spectrometer (EDAX) attachment. High resolution transmission electron microscopy (HRTEM) measurements were carried out using a 300 kV JEOL JEM 300 UHR electron microscope with a LaB_6 electron source and equipped with Semi STEM and EDX. EDX measurements were performed with an Oxford Instruments EDX detector. INCA software was used for evaluation of EDX measurements. The samples for electron microscopy were prepared dispersing the powder in ethanol and applying a drop of very dilute suspension on carbon coated grids. The suspensions were dried by slow evaporation at ambient temperature.

Differential scanning calorimetry (DSC) curves were recorded in air (100 cm^3 min^{-1}) on a simultaneous TG/DSC Instrument (Q600 SDT, TA Instruments, Crawley, UK). The experiments were performed at a heating/cooling rate of 10 ºC min^{-1} from 250ºC to 850ºC in open alumina pans. The use of platinum pans has been avoided because it is well known that platinum and bismuth react to form different alloys at different temperatures.[55, 56] Dilatometric measurements were recorded in pellets using a Linseis TMA model PT1000 in air using 10 ºC min^{-1} heating rate. The pellets were prepared from as milled powders, pressed into discs of 6 mm in diameter and ~2 mm in thickness by uniaxial pressing at 0.93 GPa and annealed at 850ºC, yielding a density of about 92%, as measured by Archimedes' method.

Dielectric measurements (dielectric constant and dielectric loss) as a function of temperature were performed using a 4263B LCR meter.[50] For these measurements pellets were prepared following the same procedure as described for the dilatometric measurements.

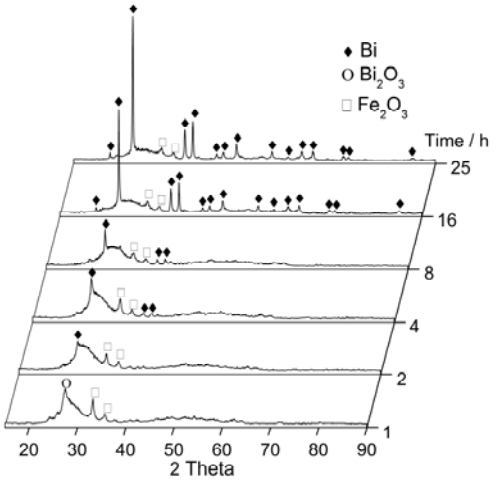

Fig. 1. Diffraction patterns of the solids obtained after milling the stoichiometric amounts of the single oxides for different periods of time in static air under experimental conditions 1 (table 1).

Results and discussion

Fig. 1 shows the diffraction patterns of the solids obtained after milling the stoichiometric amounts of the single oxides for different periods of time in static air under experimental conditions 1 (table 1). It is important to take into account that each diffraction pattern shows the result of a unique experiment, thus the jars were only opened once the desired milling time was reached and, then, the diffraction patterns were recorded. Hence, the powder-to-ball ratio and the atmosphere in the jar were not modified during the experiment. From Fig. 1, it is clear that after only one hour of milling, the crystalline structure of the pristine oxides was partially destroyed, as expected for a high energy mechanical treatment. The diffraction pattern corresponding to two hours milling shows the presence of metallic bismuth. As milling time increases, the peaks of metallic bismuth become more intense, while the peaks of bismuth oxide totally disappear. Other authors have reported the presence of metallic bismuth when intending to prepare $BiFeO_3$ by mechanosynthesis.[57]

The influence of the atmosphere on the reaction products was inferred from experiments performed in nitrogen and in oxygen (both at 7 bar), under otherwise identical conditions as those used for the experiment in Fig. 1 (experimental conditions 1 in table 1). For the experiment in nitrogen, XRD results (Fig. S1†) were identical to those observed for static air. Thus, these results suggest that for the experiments in static air or nitrogen, bismuth

oxide was reduced to metallic bismuth by the iron of the milling elements, which oxidize to iron oxide as shown in the following redox reaction:

$$Bi_2O_3 + 2Fe \rightarrow 2Bi + Fe_2O_3 \quad (1)$$

in agreement with the observations of Mozaffari et al[58] that have shown the reduction of bismuth oxide to bismuth by milling with metallic iron. Thus, this redox reaction has prevented the formation of $BiFeO_3$.

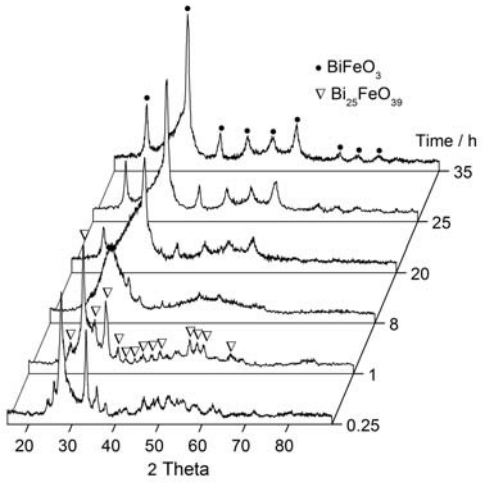

Fig. 2. Diffraction patterns of the solids obtained after milling the stoichiometric amounts of the single oxides for different periods of time in oxygen (7 bar) under experimental conditions 1 (table 1).

On the other hand, experiment in oxygen showed quite different results as illustrated by the XRD patterns of the resulting solids (Fig. 2). Thus, after the initial amorphization of the oxides, for 1 hour milling treatment, the presence of the $Bi_{25}FeO_{39}$ (sillenite) phase was observed. As grinding proceeds, this new phase was amorphisized and, eventually, the sample evolved to the desired $BiFeO_3$ perovskite phase, which was totally formed after 25 hours of milling. The nanostructured character of the sample could be inferred from the broad X-ray diffraction peaks (Fig. 2). Further grinding treatments up to 35 hours did not produce modifications in the products as indicated by XRD results (Fig. 2). Thus, even the peak widths were identical for the XRD patterns corresponding to the samples ground for 25 and 35 hours, indicating that the crystallite sizes remain unchanged. A change in the oxygen pressure in the range from 1 to 20 bar produced identical results as those reported in Fig. 2. For all the final milling products obtained under oxygen atmosphere, the X-ray fluorescence analysis yielded a Fe/Bi atomic ratio of one, while chromium was not detected in the samples, indicating that there is not relevant contamination from jar and balls. These results showed that oxygen acts as an inhibitor of the bismuth reduction by the iron from the grinding media. Moreover, oxygen may have played a role as stabilizer of the $BiFeO_3$ as it has been claimed in literature by different authors.[37, 42] Thus, all further milling experiments were performed in oxygen.

Fig. 3 shows the evolution of the minimum milling time required to obtain the pure $BiFeO_3$ perovskite phase as a function of the milling power. Several authors have derived kinematic equations to describe the velocity of the balls in the milling jar.[59-62] Thus, the impact energy (ΔE), defined as the energy transfer to the reactants in every hit, can be calculated from the following equation:

$$\Delta E = -m\left[Wv^3\frac{Rv-Rb}{Wp} + WpWvRp\right][Rv - Rb] \quad (2),$$

where m is the ball mass, Wv is the rotational speed of the vial, Wp is the rotational speed of the supporting disk, Rv is the radius of the vial, and Rb is the radius of the balls. In real systems, there is a hindering effect of the balls that decreases the impact energy. Thus, considering the hindering factor, φ, the corrected impact energy, ΔE^*, can be determined from the following equation:[59]

$$\Delta E^* = \varphi\, \Delta E \quad (3).$$

The total power transferred to the sample during the milling experiment by the collisions can be described as follows:

$$P = \Delta E^*\, N\, f \quad (4),$$

being N the number of balls into the jar and f is the frequency with which balls are launched, i.e. $f = K(Wp - Wv)/2\pi$, where K is a constant that depends on ball diameter and mill geometry.[62] Values of corrected impact energies and power for the different milling conditions used here are presented in Table 1.

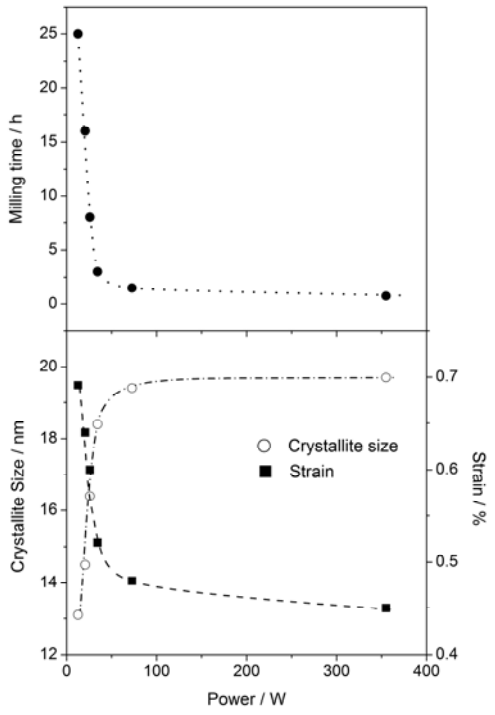

Fig.3. Evolution of the minimum milling time required to obtain the pure BiFeO3 perovskite phase and of the crystallite size of the resulting materials as a function of the milling power.

Results in Fig. 3, show a clear influence of the power on the minimum reaction time required for the preparation of the pure $BiFeO_3$ perovskite phase. Thus, while for a milling power of 12.6 W (milling conditions 1 in table 1) a reaction time of 25 hours is required, for the largest power here used (355 W, milling conditions 6) this time is reduced to about 45 minutes. The

microstructure of the products is also influenced by the milling power (Fig. 3). Thus, for a milling power of 12.6 W (milling conditions 1), the crystallite size of the $BiFeO_3$ is 13.1 nm and the strain 0.69%. An increase in the power to 20.6 W (milling conditions 2), produces a rise of the crystallite size to 14.5 nm and a decrease of the microstrain to 0.64%. Moreover, a milling power increase up to 25.8 W (milling conditions 3), produces a $BiFeO_3$ with an average crystallite size of 16.4 nm and a strain of 0.60%. Further increase in the milling power induces a significant change in the crystallite size to about 20 nm, and a reduction in the strain to about 0.45%. Interestingly, the reaction mechanism does not seem to change with the milling power.

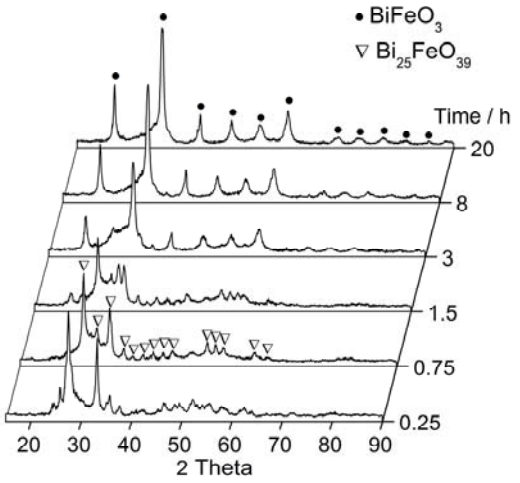

Fig.4. Diffraction patterns of the solids obtained after milling oxides for different periods of time under oxygen atmosphere for milling conditions 3 (table 1).

Fig. 4 includes the diffraction patterns of the solids obtained after milling oxides for different periods of time in oxygen atmosphere for milling conditions 3, which corresponds to a milling power of 25.8 W. Fig. 2 and 4 show identical reaction mechanisms for both 1 and 3 milling conditions, except for the reaction times required to achieve certain step. Thus, after an initial amorphization of the bismuth and iron oxides, it is observed the presence of the $Bi_{25}FeO_{39}$ intermediate phase, which is eventually converted into $BiFeO_3$ perovskite phase. Nevertheless, the kinetics of the reaction is much faster for milling conditions 3 than for milling conditions 1 and the reaction time required to produce the perovskite phase is reduced from 25 to 8 hours. It is worth noting, that, as it was observed for milling conditions 1 (Fig. 2), once the $BiFeO_3$ perovskite is formed, further milling up to 20 hours does not produce any change in the diffraction pattern of the products. Diffraction patterns of the products obtained after milling under experimental conditions 2, 4, 5 and 6 in table 1 (Fig S2†) also show that the final product is $BiFeO_3$ perovskite in all cases.

Fig. 5 includes the evolution of the specific surface area of the powders milled under milling conditions 3 as a function of the milling time. The kinetics of mechanochemical reactions have been widely studied by the changes of the specific surface area.[46] In the first stages of the reaction a progressive growth of the surface area is expected during the activation of the reagents. Then, the plastic deformation of the particles is developed and finally, the crystallization of the products as well as repeated amorphization is achieved, and the specific surface area decreases for high energy ball milling.[63] This behaviour has been observed for different kind of samples.[64, 65] Moreover, a strong correlation between the variations undergone by the specific surface and the structural changes calcite ↔aragonite during the grinding of calcium carbonate has been also reported in literature.[66]

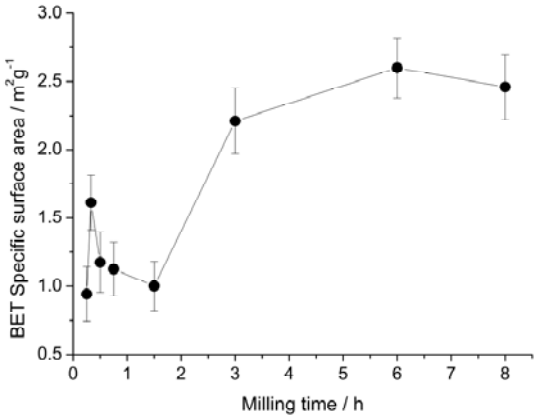

Fig.5. Variation of the specific surface as a function of grinding time under milling conditions 3 (table 1).

During the mechanosynthesis of $BiFeO_3$ (Fig. 5), the specific surface area suffers an increase in the first steps of the milling process up to about 20 minutes of treatment that corresponds to the amorphization of the original oxides, followed by a sharp decrease of the specific surface as the new sillenite phase is formed. Then, the specific surface area increases for treatment times longer than two hours, corresponding to the starting of the formation of the perovskite phase, reaching a final surface area of about 2.4 m^2g^{-1} after 8 hours of treatment.

Raman spectrum for the $BiFeO_3$ powder obtained under milling conditions 3 is shown in Fig. 6. A rhombohedral R3c structure gives rise to 13 Raman active modes: 4A1 + 9E. The spectrum obtained clearly presents 10 lines, three of them belonging to A1 modes at 170, 225 and 415 cm^{-1}, and seven from E modes at 263, 293, 355, 372, 472, 525 and 618 cm^{-1}. These values are in the range of those obtained by other authors for this material. Thus, Szafraniak et al observed, for mechanosynthetized $BiFeO_3$, bands at approximately the same values for the A1 and E modes, but they observed one band at 137 cm^{-1} that was not observed in our samples excited by a green laser (532.14 nm) and they do not studied modes above 500 cm^{-1}.[24] Kothari et al and Singh et al studied samples prepared by solid state reaction and epitaxial films respectively. They found Raman modes shifted in general at lower positions than the observed in our mechanosynthetized samples,[33, 67] while the bands observed by Fukumura et al for single crystals are shifted to higher positions with the exception of the E mode that they observed at 525 cm^{-1} and in our samples appears at 618 cm^{-1}.[68] Our results are also in good agreement with those obtained by Yuan et al for samples prepared by rapid liquid-phase sintering.[69] The absence of some bands, its broadening and small discrepancies in the positions could be related with the strain existing in the nanoparticles due to the mechanosynthesis process, as has been suggested by Szafraniak et al. These Raman spectroscopy results confirm the formation of the R3c phase.

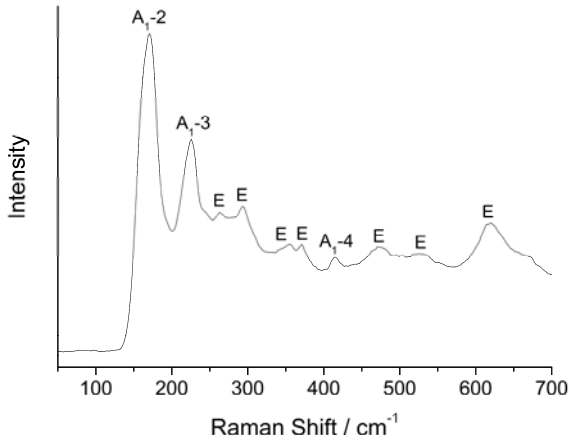

Fig.6. Raman spectrum for the BiFeO3 powder obtained under milling conditions 3 (table 1).

The morphological changes in the samples could be inferred from SEM analysis. Thus, Fig. 7 shows the SEM micrographs of the starting oxides and the powders milled during 0.25, 1.5 and 8 hours, and the EDX spectrum recorded for the final product obtained under milling conditions 3. Bismuth oxide (Fig. 7a), which has a polymeric layer structure,[70] consists of highly aggregated laminated particles, while iron oxide (Fig. 7b), which is isostructural with corundum,[71] consists of highly aggregated irregular particles. At the first stages of the mechanical treatment (Fig. 7c), bismuth oxide delaminates into single platelets mixed with the iron oxide particles. As milling proceeds and bismuth oxide reacts with iron oxide, the plate-like shape of the bismuth particles disappears and highly aggregated powders are obtained (Fig. 7d). After 8 hours of milling, when the reaction is completed as indicated by X-ray diffraction study (Fig. 4), the resulting materials consist of nanometric subunits aggregated into micron sized particles (Fig. 7e), characteristic of materials prepared by mechanical alloying. It is worth noting that SEM analysis of pure Bi_2O_3 milled under identical conditions, show the disappearing of platelets from the beginning of the grinding (Figure not shown) suggesting that the presence of Fe_2O_3 seems to be responsible of the delamination of Bi_2O_3. The analysis of the EDX spectrum of the final product (Fig. 7f) reveals that the ratio Fe/Bi equals one, as expected for stoichiometric $BiFeO_3$. The morphology of the resulting materials obtained under experimental milling conditions 1, 4, 5 and 6, as observed by SEM analysis (Fig. S3†), was very similar to that obtained under milling conditions 3 (Fig 7). Moreover, the EDX analysis indicates that all samples have a Fe/Bi ratio of 1 (Fig. S3†).

Fig. 8 shows TEM micrographs of the powder after 0.25, 0.75, 6 and 8 hours of treatment under milling conditions 3. The low-resolution micrograph at 0.25 hours (Fig. 8a) is very similar to that obtained by SEM (Fig. 7c), with laminated particles of Bi_2O_3 of approximately 100 nm mixed with smaller particles of Fe_2O_3, which are irregular in shape. In the high-resolution micrographs, the phases detected from the interlayer spaces by the lattice fringes show that the powder consists of a mixture of the starting oxides, as observed by XRD patterns (Fig. 4). As an example, the high resolution TEM micrograph in Fig. 8b shows a uniform interplanar spacing of 0.325 nm corresponding to the (-121) plane of Bi_2O_3. Fig. 8c and d illustrates the TEM study after milling during 0.75 hours. The low-resolution micrograph (Fig. 8c) shows a highly aggregated material composed of irregular particles. In the high-resolution mode (Fig. 8d), the intermediate $Bi_{25}FeO_{39}$ phase is observed with an interplanar spacing of 0.415 nm corresponding with the (211) plane, in agreement with the XRD pattern recorded for this milling time (Fig. 4). After 6 hours of milling, the reaction is almost completed and the powder is clearly more homogeneous (Fig. 8e). The high-resolution micrograph (Fig. 8f) reveals the presence of particles of $BiFeO_3$ surrounded by a thin layer of amorphous phase, in agreement with the XRD study. Finally, the TEM study after 8 hours milling (Fig. 8g) reveals that the final particles consist of aggregated nanometric subunits with an average size of 25 ± 18 nm. This latter size is very close to that obtained using the single X-ray line fitting procedure for the crystallite size of this sample, confirming that the $BiFeO_3$ subunits consist of single nanosized crystals.

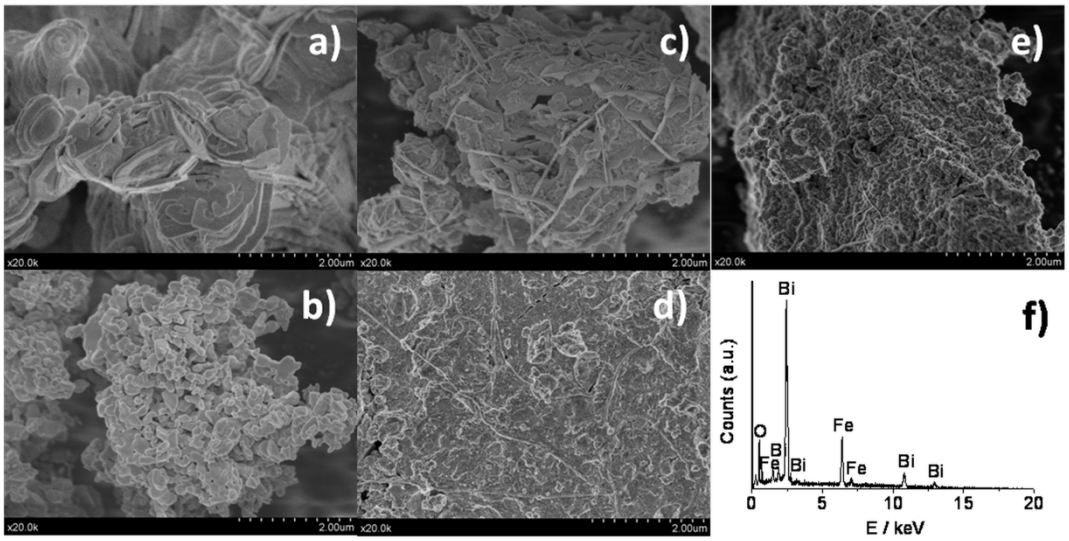

Fig.7. Scanning electron micrographs of the bismuth (a) and iron (b) starting oxides and the powders milled during 0.25 (c), 1.5 (d), 6 (e) and 8 (f) hours under milling conditions 3.

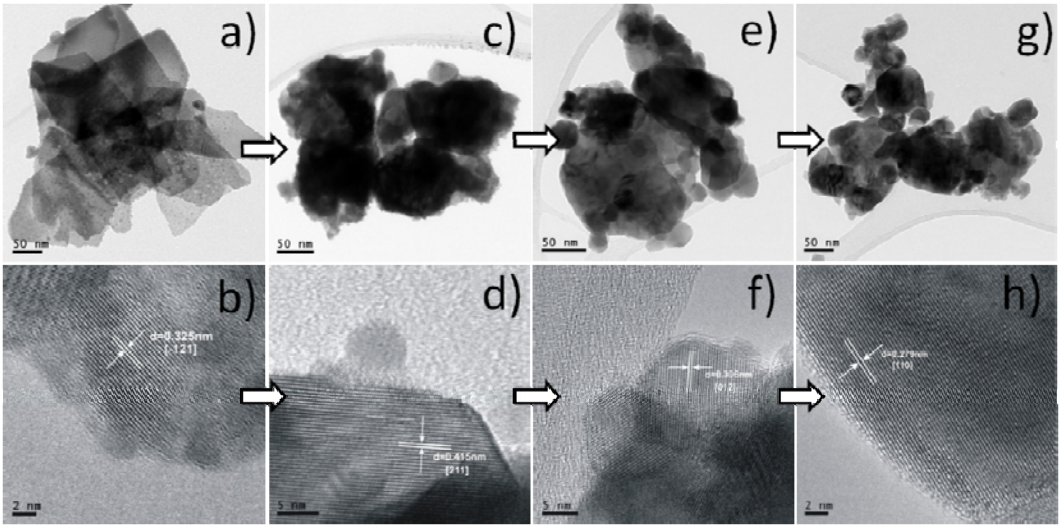

Fig.8. TEM micrographs of the powder after 0.25 (a, b), 0.75 (c, d), 6 (e, f) and 8 (g, h) hours of milling under milling conditions 3

High-resolution TEM study confirms that BiFeO3 is obtained as homogeneous nanoparticles after 8 hours of grinding under milling conditions 3. As an example, a particle with an interplanar spacing of 0.279 nm corresponding of the (110) plane of $BiFeO_3$ is presented (Fig. 8h). Besides, particles were free of any amorphous layer on the surface, unlike many materials prepared by mechanical alloying. EDX analysis (Fig. 9a) confirms a Bi/Fe atomic ratio very close to 1, as expected for $BiFeO_3$. The scattering vector versus intensity corresponding to the electron diffraction pattern in the inset for the final product after 8 hours of milling is also shown in Fig. 9b. This pattern is identical to that obtained by XRD (Fig. 4) demonstrating that the final product is the desired phase $BiFeO_3$. TEM, EDX and SAED analysis of samples obtained under other milling conditions show a similar behaviour (Fig. S4† and S5†).

XRF analyses show, for all samples, that the ratio Fe/Bi = 1 of the starting mixture is maintained all over the grinding process, in agreement with the EDX observations. It would be expected that, if a significant amount of iron were incorporated to the ground product from the milling media, such a ratio would increase, contrarily to our experimental observations. Moreover, if we bear in mind that the grinding media is made of chromium steel, a contamination with chromium would necessarily occur if material from the grinding media were incorporated into the milled product, while this metal has not been detected. These results suggest that the effect of the oxygen atmosphere is just to inhibit the reaction between bismuth oxide and the iron of the grinding media avoiding the reduction of this oxide.

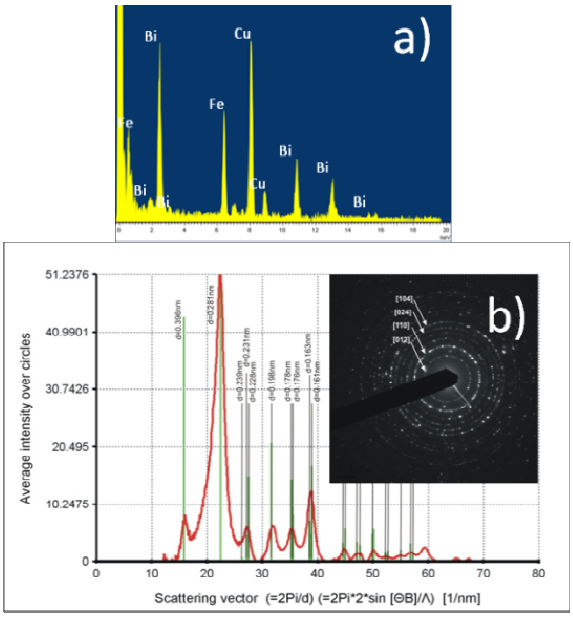

Fig.9. EDX analysis (a) and scattering vector versus intensity corresponding to the electron diffraction pattern shown in the inset (b) of the final product after 8 hours of milling under milling conditions 3.

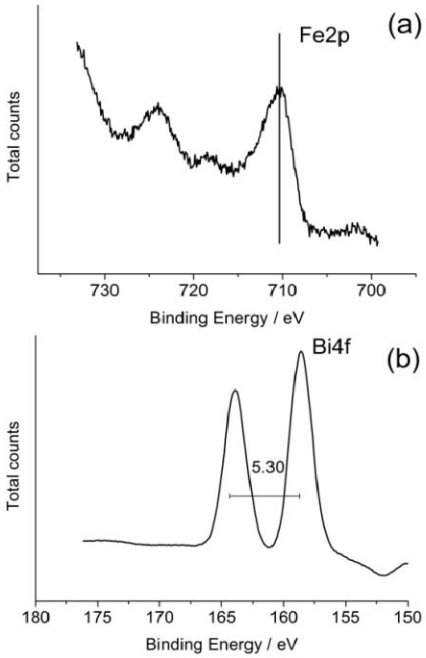

Fig.10. XPS spectra for Fe2p (a) and for Bi4f (b) for the sample milled 0.5 hours under milling conditions 3.

X-ray photoelectron spectroscopy (XPS) is very sensitive to the chemical composition of the outermost layers. Fig. 10 shows, as a way of example, the spectrums for Fe2p (Fig. 10a) and for Bi4f (Fig. 10b) for the sample milled 0.5 hours under milling conditions 3. Measured binding energies are in the range of those reported for Fe^{+3} and Bi^{+3},[72, 73] while Fe^{+2} or Bi^{+5} ions are not detected. For this sample, the atomic ratio of bismuth to iron is approximately equal to eight, showing enrichment in bismuth in the outermost layer of this sample. This ratio decreases as the milling time increases, being one for the resulting $BiFeO_3$ obtained after 8 hours of milling (Fig S6†).

All these results support that the mechanochemical reaction between Bi_2O_3 and Fe_2O_3 takes place through a mechanism that implies the diffusion of Bi^{3+} inside the Fe_2O_3 particles. It is noteworthy to point out that Bernardo et al[74] have studied the reactivity of Fe_2O_3 and Bi_2O_3 by heating two pellets of these material previouslys pressed with a platinum mark in between to follow the diffusion process according with the Kirkendall effect, and they concluded that the reaction implies the diffusion of Bi^{3+} into the iron oxide pellet. Thus, for the mechanochemical reaction (Fig. 11), in a first step, the pristine oxides are amorphysized, as shown by XRD (Fig. 2 and 4), by the high energy of the ball impacts. Besides, bismuth oxide that has a polymeric layer structure and is the softest of the two reactants,[75, 76] coats the harder iron oxide particles. Thus, the chemical analyses show a larger concentration of bismuth species on the surface for the intermediate materials. It has been observed that as milling further continues, the diffusion of the bismuth into the hematite phase progresses and an intermediate compound, i.e. sillenite ($Bi_{25}FeO_{39}$), is formed in the interphase. The formation of this compound is observed both by XRD and high resolution TEM for all the grinding conditions investigated here, suggesting that it is a necessary step for the mechanochemical formation of the perovskite phase. The formation of sillenite as intermediate has been observed for both thermal solid-state and hydrothermal procedures.[74, 77] In this work, for the sillenite phase, it has been used the $Bi_{25}FeO_{39}$ formulae, unlike some other works that take $Bi_{25}FeO_{40}$,[39, 77, 78] because, this latter formula implies that one Bi ion takes a +5 valence, while we have not observed any Bi^{5+} ions in the XPS measurements. As milling continues, it produces amorphization of the sillenite phase followed by the formation of the final perovskite phase.

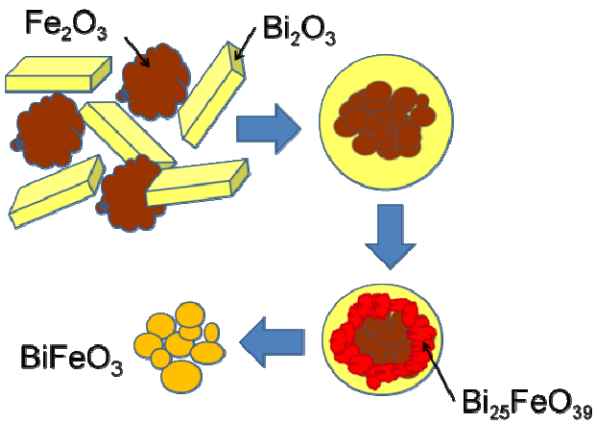

Fig.11. Schematic diagram of the mechanism for the mechanochemical reaction.

The electron microscope study shows that the final product consists of nanometric crystals aggregated into larger units, while amorphous phases, commonly observed for ground materials on the surface of the particles, were not detected in this case. The formation of aggregates in materials obtained by mechanical alloying is a very general observation and it has been explained in terms of a cold-welding mechanism produced by the "extra-energy" stored by the strains induced by lattice imperfections generated during grinding.[79-82] Thus, the resulting aggregates are formed by small crystallites welded into a mosaic structure where the grain boundaries are the main contribution to the microstrains.[80, 82] The reverse relationship between the average crystallite size and microstrains percentage shown in Fig. 3 supports this conclusion.

For the sake of comparison of the mechanisms of mechanochemical reaction and conventional thermal solid state reaction, Fig. 12 includes a set of XRD patterns obtained for the products of the solid state reaction at different temperatures in air. Thus, for the lowest temperature, i.e. 600ºC, a mixture of $BiFeO_3$ and $Bi_{25}FeO_{39}$ phases is detected. As temperature increases up to 750ºC, the percentage of the $Bi_{25}FeO_{39}$ phase decreases while that of the $BiFeO_3$ increases, indicating that $Bi_{25}FeO_{39}$ is an intermediate for the synthesis of $BiFeO_3$ perovskite, in a similar way that it was observed for the mechanochemical reaction described above. At 800ºC, in addition to $BiFeO_3$ and $Bi_{25}FeO_{39}$, a new phase, i.e. mullite ($Bi_2Fe_4O_9$), is present. At temperatures higher than 800ºC (pattern not shown), the percentage of unwilling phases increased. Thus, by conventional thermal solid state reaction, the presence of impurities could not be avoided in the entire range of investigated temperatures. This observation is in agreement with previous results published in literature, where it has been claimed that the formation of $BiFeO_3$ and the crystallization of $Bi_2Fe_4O_9$ mullite particles take place simultaneously, and even changing experimental conditions such as heating conditions or using co-precipitated samples could not avoid the formation of unwilling phases.[74] Thus, a further purification step, for example by acid treatment, is required to purify the powders obtained by conventional thermal solid-state reaction, while this treatment might change the stoichiometry of the system and/or dissolve part of the perovskite phase.

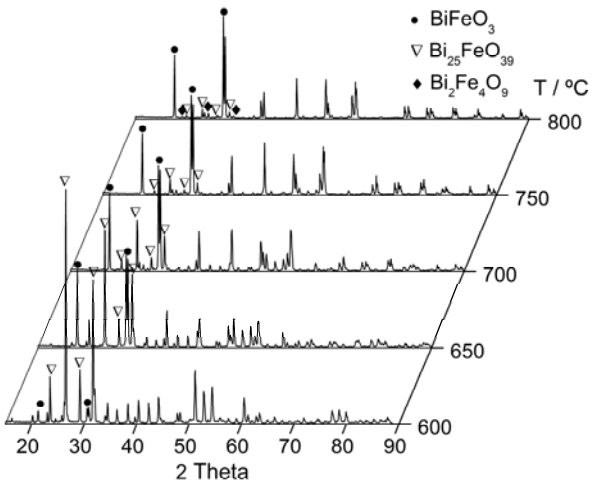

Fig.12. Diffraction patterns obtained for the products of the Bi_2O_3 + Fe_2O_3 solid state reaction at different temperatures in air.

In contrast, the XRD pattern corresponding to the sample ground for eight hours under milling conditions 3 and heated to 850ºC corresponds to pure $BiFeO_3$ phase (Fig. 13), as confirmed by Rietveld refinement using an R3c space group. The calculated pattern clearly fits the experimental data even at high values of theta, providing the goodness of the refinement. The cell parameters, atomic coordinates, thermal isotropic factors, and discrepancy factors obtained are shown in Table 2. Structural data is in agreement with previously reported results for $BiFeO_3$ prepared by means of other methods.[18, 21, 83] The inset (Fig. 13) shows the unit cell calculated using the cell parameters obtained by the refinement.

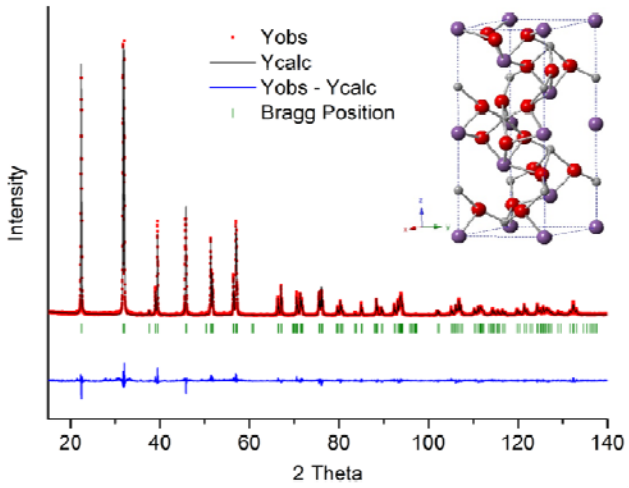

Fig.13. Diffraction pattern corresponding to the sample ground for eight hours under milling conditions 3 and heated to 850ºC (dots). The solid lines are the results of the Rietveld refinement. The inset shows the resulting unit cell.

Table 2. Rietveld refinement structural parameters from an XRD patter corresponding to the sample ground for eight hours under milling conditions 3 and heated to 850ºC.

Cell parameters (Å)						
a = 5.5798(5)		b = 5.5798(5)		c = 13.8724(1)		
α = 90º		β = 90º		γ = 120º		
Atomic parameters						
	Wyckoff site	x	y	z	Biso	Mult.
Bi	6a	0.00000	0.00000	0.00000	0.309	6
Fe	6a	0.00000	0.00000	0.22067	0.310	6
O	18b	0.44511	0.01262	0.95238	0.346	18
Discrepancy factors						
R_p: 6.66		R_{wp}: 9.26		R_{exp}: 6.00		χ^2: 2.38

The DSC measurements show the multiferroic character of the prepared samples. Thus, Fig. 14a includes, as an example, the DSC of the as ground powders obtained under milling conditions 3. The DSC trace shows two endothermic peaks. The first one is a weak peak at 367 ºC corresponding to the Néel temperature (T_N, antiferromagnetic-paramagnetic transition), while the second one is a more intense peak at 828 ºC corresponding to the Curie temperature (T_C, ferroelectric-paraelectric transition). The same peaks have been observed on the DSC plot in Fig. 14b corresponding to the sample obtained under milling conditions 3 and heated at 850ºC, supporting that the powders directly obtained by grinding are constituted by pure $BiFeO_3$ according with the results above reported. The smaller crystallite size of the as ground powders explains the broadening of the peaks as compared with that of the heated sample. The values of T_N and T_C are in good agreement with previous reports.[13, 38, 84, 85] The cooling ramp shows the reversibility of both transitions and the enthalpy associated is 3.50 ± 0.50 kJ mol^{-1} for the ferroelectric transition. The thermomechanical curve of a dense (>92%) pellet prepared by sintering of the sample obtained under milling conditions 3 at 850ºC, also shows the reversible ferroelectric transition as a large negative thermal expansion at T_C (Fig. 14c), in agreement with DSC results shown above.

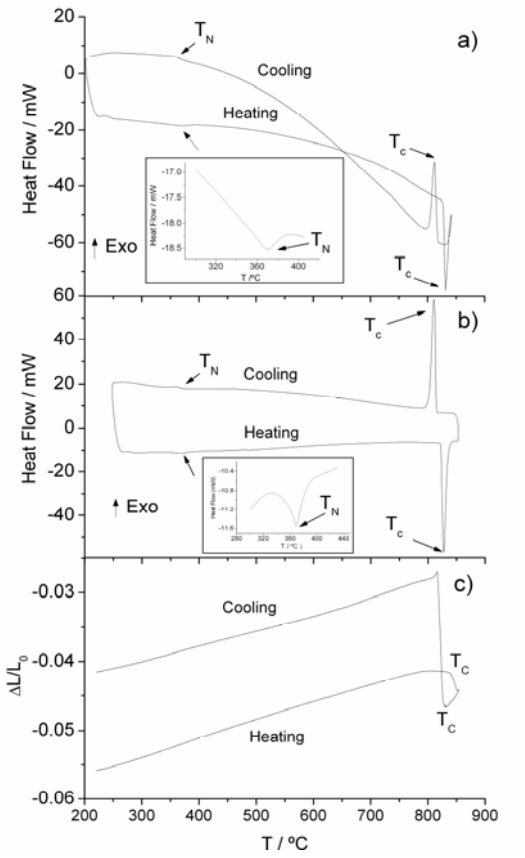

Fig.14. (a) DSC corresponding to the sample obtained under milling conditions 3 and heated at 850ºC. (b) Dilatometric curve of a dense (>92%) pellet prepared by sintering of the sample obtained under grinding conditions 3 at 850ºC.

Fig. 15 includes the evolution of the dielectric constant and the dielectric loss as a function of the temperature at different frequencies for a dense (>92%) pellet prepared by sintering of the sample obtained under grinding conditions 3 at 850ºC. The values of the dielectric constant at room temperature were 100.7, 93.1 and 84.8 for 1 kHz, 10 kHz and 100 kHz, respectively. Additionally, Fig. 15a shows for the dielectric constant an increase with temperature and a decrease with the frequency. Moreover, Fig. 15b shows very low values of tan δ up to about 200 ºC. These results clearly show that the sample is a good electrical insulator up to 200ºC as expected for high quality $BiFeO_3$ material.[5, 38] Thus, the proposed method allows obtaining materials with excellent electrical properties. This is a very interesting characteristic of the prepared samples, as far as it has

been recognized the difficulties in preparing insulating $BiFeO_3$ materials due to presence of secondary phases or oxygen vacancies that yield semiconductivity at room temperature causing high leakage currents.[34, 86-88] A detailed analysis of the electrical properties of these samples by impedance spectroscopy has been carried out elsewhere.[89]

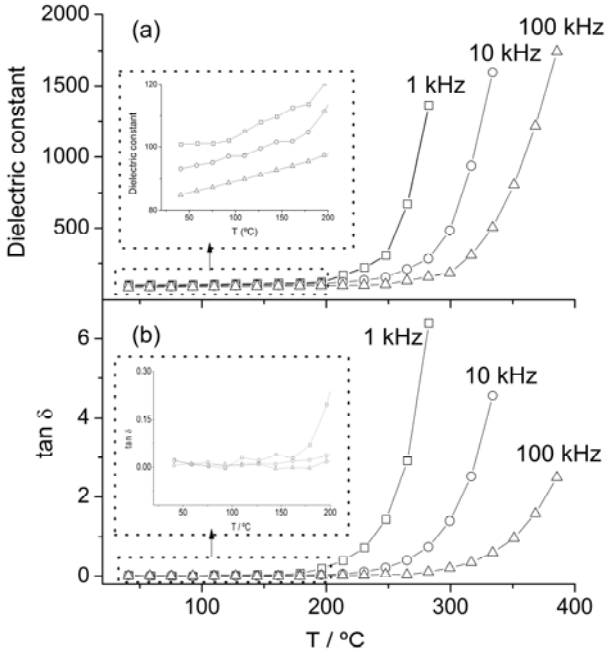

Fig.15. Evolution of the dielectric constant (a) and dielectric loss (b) as a function of the temperature at different frequencies for a pellet prepared by sintering of the sample obtained under grinding conditions 3 at 850ºC.

Conclusions

It has been shown that direct mechanochemical reaction allows obtaining pure nanostructured $BiFeO_3$ perovskite by grinding pure Fe_2O_3 and Bi_2O_3 in oxygen atmosphere at reaction times even smaller than 50 minutes. The crystallite size of the material could be tailored by selecting the proper milling conditions, in particular the milling power. Thus, particles in the range from about 13 to 20 nm could be obtained. The mechanism of the reaction has been studied, concluding that the reaction involves at the first stages of the high-energy milling, the coating of the Fe_2O_3 particles by Bi_2O_3 followed by the diffusion of the bismuth into the iron oxide to produce an intermediate, i.e. $Bi_{25}FeO_{39}$. As milling proceeds, the pure perovskite phase is formed. The nanoparticles obtained has been annealed or sintered without the formation of unwilling phases such as mullite. This is a significant difference with other methods that produce some amount of unwilling phases that should be somehow removed. The multiferroic character of the prepared material was observed by DSC measurements that have shown both the ferroelectric and ferromagnetic transitions at 367ºC and 828ºC, respectively. The electrical characterization (dielectric constants and dielectric losses) of the prepared sample have shown it is a good electrical insulator up to 200ºC as expected for high quality $BiFeO_3$ material.

Acknowledgments

We thank Spanish Government (project CTQ 2011-27626), Junta de Andalucía (projects TEP-03002 and TEP-7858) and FEDER funds for financial support.

References

1. W. Eerenstein, N. D. Mathur and J. F. Scott, *Nature*, 2006, **442**, 759-765.
2. M. Fiebig, *Journal of Physics D-Applied Physics*, 2005, **38**, R123-R152.
3. N. A. Spaldin and M. Fiebig, *Science*, 2005, **309**, 391-392.
4. D. I. Khomskii, *Journal of Magnetism and Magnetic Materials*, 2006, **306**, 1-8.
5. G. Catalan and J. F. Scott, *Advanced Materials (Weinheim, Germany)*, 2009, **21**, 2463-2485.
6. C. Ederer and N. A. Spaldin, *Physical Review B*, 2005, **71**.
7. P. Fischer, M. Polomska, I. Sosnowska and M. Szymanski, *Journal of Physics C-Solid State Physics*, 1980, **13**, 1931-1940.
8. J. M. Moreau, C. Michel, R. Gerson and W. J. James, *Journal of Physics and Chemistry of Solids*, 1971, **32**, 1315-&.
9. J. M. Caicedo, J. A. Zapata, M. E. Gomez and P. Prieto, *Journal of Applied Physics*, 2008, **103**.
10. K. S. Nalwa, A. Garg and A. Upadhayaya, *Indian Journal of Engineering and Materials Sciences*, 2008, **15**, 91-94.
11. M. Valant, A. K. Axelsson and N. Alford, *Chemistry of Materials*, 2007, **19**, 5431-5436.
12. S. M. Selbach, M. A. Einarsrud and T. Grande, *Chemistry of Materials*, 2009, **21**, 169-173.
13. S. M. Selbach, T. Tybell, M. A. Einarsrud and T. Grande, *Advanced Materials (Weinheim, Germany)*, 2008, **20**, 3692-3696.
14. Y. Zhang, A. M. Schultz, P. A. Salvador and G. S. Rohrer, *Journal of Materials Chemistry*, 2011, **21**, 4168-4174.
15. S. Ghosh, S. Dasgupta, A. Sen and H. S. Maiti, *Journal of the American Ceramic Society*, 2005, **88**, 1349-1352.
16. A. Hardy, S. Gielis, H. Van den Rul, J. D'Haen, M. K. Van Bael and J. Mullens, *Journal of the European Ceramic Society*, 2009, **29**, 3007-3013.
17. Q. H. Jiang, C. W. Nan, Y. Wang, Y. H. Liu and Z. J. Shen, *Journal of Electroceramics*, 2008, **21**, 690-693.
18. S. M. Selbach, M. A. Einarsrud, T. Tybell and T. Grande, *Journal of the American Ceramic Society*, 2007, **90**, 3430-3434.
19. S. M. Selbach, T. Tybell, M. A. Einarsrud and T. Grande, *Chemistry of Materials*, 2007, **19**, 6478-6484.
20. J. H. Xu, H. Ke, D. C. Jia, W. Wang and Y. Zhou, *Journal of Alloys and Compounds*, 2009, **472**, 473-477.
21. T. T. Carvalho and P. B. Tavares, *Mater. Lett.*, 2008, **62**, 3984-3986.
22. V. Fruth, L. Mitoseriu, D. Berger, A. Ianculescu, C. Matei, S. Preda and M. Zaharescu, *Progress in Solid State Chemistry*, 2007, **35**, 193-202.
23. D. Maurya, H. Thota, K. S. Nalwa and A. Garg, *Journal of Alloys and Compounds*, 2009, **477**, 780-784.
24. I. Szafraniak, M. Polomska, B. Hilczer, A. Pietraszko and L. Kepinski, *Journal of the European Ceramic Society*, 2007, **27**, 4399-4402.

25. C. Correas, T. Hungria and A. Castro, *Journal of Materials Chemistry*, 2011, **21**, 3125-3132.
26. K. L. Da Silva, D. Menzel, A. Feldhoff, C. Kubel, M. Bruns, A. Paesano, A. Duvel, M. Wilkening, M. Ghafari, H. Hahn, F. J. Litterst, P. Heitjans, K. D. Becker and V. Sepelak, *Journal of Physical Chemistry C*, 2011, **115**, 7209-7217.
27. C. Chen, J. R. Cheng, S. W. Yu, L. J. Che and Z. Y. Meng, *Journal of Crystal Growth*, 2006, **291**, 135-139.
28. Y. G. Wang, G. Xu, Z. H. Ren, X. Wei, W. J. Weng, P. Du, G. Shen and G. R. Han, *Journal of the American Ceramic Society*, 2007, **90**, 2615-2617.
29. Z. Li, Y. Shen, C. Yang, Y. Lei, Y. Guan, Y. Lin, D. Liu and W. Nan, *Journal of Materials Chemistry A*, 2013, **1**, 823-829.
30. C.-J. Tsai, C.-Y. Yang, Y.-C. Liao and Y.-L. Chueh, *Journal of Materials Chemistry*, 2012, **22**, 17432-17436.
31. J. Chen, X. R. Xing, A. Watson, W. Wang, R. B. Yu, J. X. Deng, L. Yan, C. Sun and X. B. Chen, *Chemistry of Materials*, 2007, **19**, 3598-3600.
32. X. B. He and L. A. Gao, *Ceramics International*, 2009, **35**, 975-978.
33. D. Kothari, V. R. Reddy, V. G. Sathe, A. Gupta, A. Banerjee and A. M. Awasthi, *Journal of Magnetism and Magnetic Materials*, 2008, **320**, 548-552.
34. A. K. Pradhan, K. Zhang, D. Hunter, J. B. Dadson, G. B. Loiutts, P. Bhattacharya, R. Katiyar, J. Zhang, D. J. Sellmyer, U. N. Roy, Y. Cui and A. Burger, *Journal of Applied Physics*, 2005, **97**.
35. S. H. Xie, J. Y. Li, R. Proksch, Y. M. Liu, Y. C. Zhou, Y. Y. Liu, Y. Ou, L. N. Lan and Y. Qiao, *Applied Physics Letters*, 2008, **93**.
36. J. Wei and D. Xue, *Materials Research Bulletin*, 2008, **43**, 3368-3373.
37. G. L. Yuan, S. W. Or, Y. P. Wang, Z. G. Liu and J. M. Liu, *Solid State Communications*, 2006, **138**, 76-81.
38. R. Palai, R. S. Katiyar, H. Schmid, P. Tissot, S. J. Clark, J. Robertson, S. A. T. Redfern, G. Catalan and J. F. Scott, *Physical Review B*, 2008, **77**.
39. J. Lu, L. J. Qiao, P. Z. Fu and Y. C. Wu, *Journal of Crystal Growth*, 2011, **318**, 936-941.
40. M. I. Morozov, N. A. Lomanova and V. V. Gusarov, *Russian Journal of General Chemistry (Translation of Zhurnal Obshchei Khimii)*, 2003, **73**, 1676-1680.
41. H. Bea, M. Bibes, A. Barthelemy, K. Bouzehouane, E. Jacquet, A. Khodan, J. P. Contour, S. Fusil, F. Wyczisk, A. Forget, D. Lebeugle, D. Colson and M. Viret, *Applied Physics Letters*, 2005, **87**.
42. S. M. Selbach, T. Tybell, M. A. Einarsrud and T. Grande, *Journal of Solid State Chemistry*, 2010, **183**, 1205-1208.
43. T. J. Park, G. C. Papaefthymiou, A. J. Viescas, A. R. Moodenbaugh and S. S. Wong, *Nano Letters*, 2007, **7**, 766-772.
44. R. Mazumder, P. S. Devi, D. Bhattacharya, P. Choudhury, A. Sen and M. Raja, *Applied Physics Letters*, 2007, **91**.
45. S. Goswami, D. Bhattacharya, P. Choudhury, B. Ouladdiaf and T. Chatterji, *Applied Physics Letters*, 2011, **99**.
46. P. Balaz, *Mechanochemistry in Nanoscience and Minerals Engineering*, 2008.
47. C. Suryanarayana, *Progress in Materials Science*, 2001, **46**, 1-184.
48. L. B. Kong, T. S. Zhang, J. Ma and F. Boey, *Progress in Materials Science*, 2008, **53**, 207-322.
49. J. M. Xue, J. Wang and D. M. Wan, *Journal of the American Ceramic Society*, 2000, **83**, 232-234.
50. P. E. Sanchez-Jimenez, L. A. Perez-Maqueda, M. J. Dianez, A. Perejon and J. M. Criado, *Composite Structures*, 2010, **92**, 2236-2240.
51. L. B. Kong, W. Zhu and O. K. Tan, *Journal of Materials Science Letters*, 2000, **19**, 1963-1966.
52. A. R. James, B. Rao, M. Pathak, S. V. Kamat and J. Subrahmanyam, *Nanotechnology*, 2008, **19**.
53. H. M. Rietveld, *Journal of Applied Crystallography*, 1969, **2**, 65-&.
54. J. Rodriguez-Carvajal, *Short Reference Guide of the FullProf. Prog., Version 3.5, Laboratory Leon Brilloium (CEA-CNRS)*, 1997.
55. H. Okamoto, *Journal of Phase Equilibria*, 1991, **12**.
56. T. Atsuki, N. Soyama, T. Yonezawa and K. Ogi, *Japanese Journal of Applied Physics Part 1-Regular Papers Short Notes & Review Papers*, 1995, **34**, 5096-5099.
57. E. Markiewicz, B. Hilczer, M. Błaszyk, A. Pietraszko and E. Talik, *Journal of Electroceramics*, 2011, **27**, 154-161.
58. M. Mozaffari, J. Amighian and A. Hasanpour, *Physica B-Condensed Matter*, 2006, **371**, 309-312.
59. N. Burgio, A. Iasonna, M. Magini, S. Martelli and F. Padella, *Nuovo Cimento Soc. Ital. Fis. D-Condens. Matter At. Mol. Chem. Phys. Fluids Plasmas Biophys.*, 1991, **13**, 459-476.
60. T. Rojac, M. Kosec, B. Malič and J. Holc, *Journal of the European Ceramic Society*, 2006, **26**, 3711-3716.
61. M. Abdellaoui and E. Gaffet, *Acta Metall. Mater.*, 1995, **43**, 1087-1098.
62. M. Magini, C. Colella, A. Iasonna and F. Padella, *Acta Mater.*, 1998, **46**, 2841-2850.
63. E. G. Avvakumov, Senna, M. and Kosova, N., *Soft Mechanochemical Synthesis. A Basis for New Chemical Technologies*, Kluwer Academic Publishers, Boston, 2001.
64. V. Balek, L. A. Perez-Maqueda, J. Poyato, Z. Cerny, V. Ramirez-Valle, I. M. Buntseva and J. L. Perez-Rodriguez, *Journal of Thermal Analysis and Calorimetry*, 2007, **88**, 87-91.
65. J. Subrt, L. A. Perez-Maqueda, J. M. Criado, C. Real, J. Bohacek and E. Vecernikova, *Journal of the American Ceramic Society*, 2000, **83**, 294-298.
66. J. M. Criado and J. M. Trillo, *Journal of the Chemical Society-Faraday Transactions I*, 1975, **71**, 961-966.
67. M. K. Singh, H. M. Jang, S. Ryu and M.-H. Jo, *Applied Physics Letters*, 2006, **88**, 042907.
68. H. Fukumura, H. Harima, K. Kisoda, M. Tamada, Y. Noguchi and M. Miyayama, *Journal of Magnetism and Magnetic Materials*, 2007, **310**, E367-E369.
69. G. L. Yuan, S. W. Or and H. L. W. Chan, *Journal of Applied Physics*, 2007, **101**.
70. N. N. GREENWOOD and A. EARNSHAW, *Chemistry of the Elements, Second Edition* Butterworth-Heineman, Oxford, UK, 1997
71. R. M. Cornell and U. Schwertmann, *The iron oxides. Structure, properties, reactions, occurrence and uses*, VCH, Weinheim (Germany), 1996.
72. V. Fruth, M. Popa, J. M. Calderon-Moreno, E. M. Anghel, D. Berger, M. Gartner, M. Anastasescu, P. Osiceanu and M. Zaharescu, *Journal of the European Ceramic Society*, 2007, **27**, 4417-4420.
73. D. Rout, K. S. Moon and S. J. L. Kang, *Journal of Raman Spectroscopy*, 2009, **40**, 618-626.

74. M. S. Bernardo, T. Jardiel, M. Peiteado, A. C. Caballero and M. Villegas, *Journal of the European Ceramic Society*, 2011, **31**, 3047-3053.
75. P. Korbel and M. Novak, *The complete encyclopedia of minerals*, Grange Books, United Kingdom, 2001.
76. R. A. B. John W. Anthony, Kenneth W. Bladh, and Monte C. Nichols, Mineralogical Society of America, Chantilly, VA 20151-1110, USA, 1997, vol. 3.
77. D. R. Cai, J. M. Li, T. Tong, D. R. Jin, S. W. Yu and J. R. Cheng, *Mater. Chem. Phys.*, 2012, **134**, 139-144.
78. D. C. Craig and N. C. Stephenson, *Journal of Solid State Chemistry*, 1975, **15**, 1-8.
79. L. Lu and M. O. Lai, *Mechanical Alloying*, Kluwer Academic Publishers, Boston, MA, 1998.
80. C. Real, J. M. Criado and V. Balek, *Journal of Materials Science*, 1998, **33**, 5247-5254.
81. J. M. Criado and M. J. Dianez, *Journal of Materials Science*, 1991, **26**, 821-823.
82. J. M. Criado, M. Gonzalez and C. Real, *Journal of Materials Science Letters*, 1986, **5**, 467-469.
83. A. Reyes, C. de la Vega, M. E. Fuentes and L. Fuentes, *Journal of the European Ceramic Society*, 2007, **27**, 3709-3711.
84. M. M. Kumar, V. R. Palkar, K. Srinivas and S. V. Suryanarayana, *Applied Physics Letters*, 2000, **76**, 2764-2766.
85. T. Xian, H. Yang, X. Shen, J. L. Jiang, Z. Q. Wei and W. J. Feng, *Journal of Alloys and Compounds*, 2009, **480**, 889-892.
86. Y. P. Wang, L. Zhou, M. F. Zhang, X. Y. Chen, J. M. Liu and Z. G. Liu, *Applied Physics Letters*, 2004, **84**, 1731.
87. B. Yu, M. Li, J. Liu, D. Guo, L. Pei and X. Zhao, *Journal of Physics D: Applied Physics*, 2008, **41**, 065003.
88. X. H. Zheng, P. J. Chen, N. Ma, Z. H. Ma and D. P. Tang, *Journal of Materials Science: Materials in Electronics*, 2011, **23**, 990-994.
89. A. Perejon, N. Maso, A. R. West, P. E. Sanchez-Jimenez, R. Poyato, J. M. Criado and L. A. Perez-Maqueda, *Journal of the American Ceramic Society*, 2013. **DOI:** 10.1111/jace.12186